ELSEVIER

Nuclear Instruments and Methods in Physics Research A 465 (2001) 414–427

NUCLEAR INSTRUMENTS & METHODS IN PHYSICS RESEARCH Section A

www.elsevier.nl/locate/nima

The CLAS Cherenkov detector

G. Adams[a], V. Burkert[b], R. Carl[a], T. Carstens[b], V. Frolov[a], L. Houghtlin[a], G. Jacobs[b], M. Kossov[c,b], M. Klusman[a], B. Kross[b], M. Onuk[a], J. Napolitano[a], J.W. Price[a,1], C. Riggs[b], Y. Sharabian[d], A. Stavinsky[c], L.C. Smith[e], W.A. Stephens[e], P. Stoler[a,*], W. Tuzel[b], K. Ullrich[a], A. Vlassov[c,b], A. Weisenberger[b], M. Witkowski[a], B. Wojtekhowski[a,2], P.F. Yergin[a], C. Zorn[b]

[a] *Department of Physics, Rensselaer Polytechnic Institute, Troy, NY 12180, USA*
[b] *Thomas Jefferson National Accelerator Facility, Newport News, VA 23606, USA*
[c] *Institute For Theoretical & Experimental Physics, Moscow, Russia*
[d] *Yerevan Physics Institute, Yerevan, Armenia*
[e] *Physics Department, Univ. of Virginia, Charlottesville, VA 22904, USA*

Received 11 August 2000; received in revised form 16 September 2000; accepted 24 September 2000

Abstract

The design, construction, and performance of the CLAS Cherenkov threshold gas detector at Jefferson Lab is described. The detector consists of 216 optical modules. Each module consists of three adjustable mirrors of lightweight composite construction, a Winston light collecting cone, a 5-in. photomultiplier tube, and specially designed magnetic shielding. Efficiencies and response functions have been measured. © 2001 Elsevier Science B.V. All rights reserved.

PACS: 95.55.Vj

Keywords: Detector; Cherenkov; Gas; Threshold

1. Introduction

The CEBAF Large Acceptance Spectrometer (CLAS) is a nearly-4π detector at the Thomas Jefferson National Accelerator Facility for the study of electromagnetic interactions with nucleons and nuclei. Fig. 1 schematically shows the CLAS and the placement of the various detector components.

Six superconducting coils produce a toroidal magnetic field having six-fold symmetry around the beam axis, in which charged particles are bent in θ while their ϕ direction remains largely unaffected. Tracking is accomplished in three drift chamber regions [1], containing a total of 18 axial and 16 stereo layers of drift cells. These are followed by gas Cherenkov detectors, scintillation detectors [2], and electromagnetic calorimeters [3] for particle identification and timing. The Cherenkov detectors serve the functions of triggering

*Corresponding author. Fax: +1-518-276-6680.

[1] Current address: UCLA Department of Physics and Astronomy, Los Angeles, CA 90095–1547, USA.

[2] Current address: Jefferson Laboratory, 12000 Jefferson Avenue, Newport News, VA 23606, USA.

0168-9002/01/$ - see front matter
PII: S0168-9002(00)01313-9

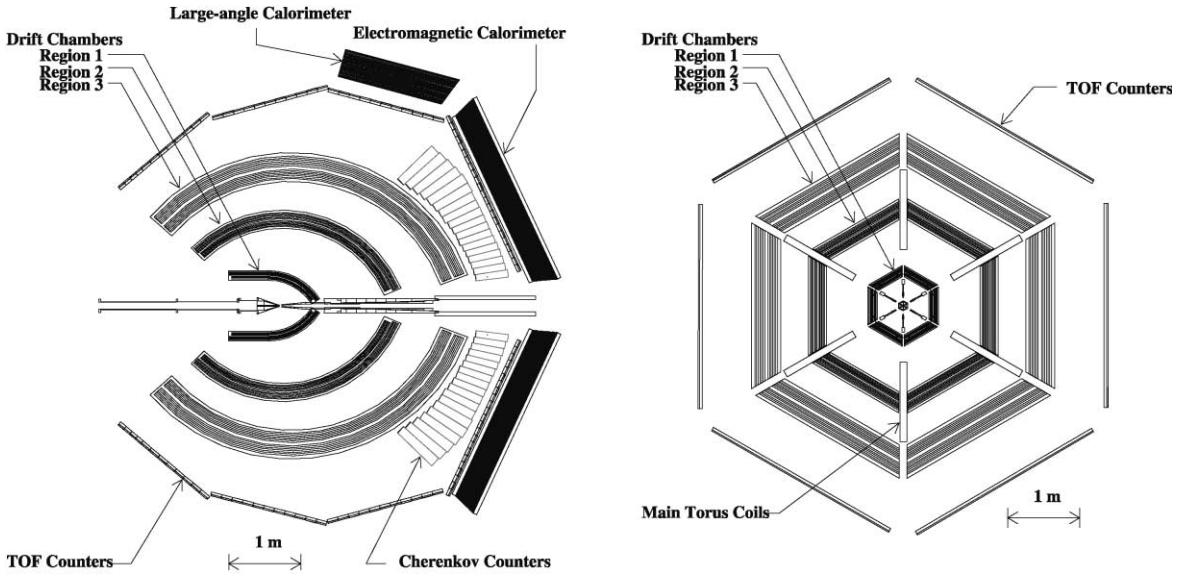

Fig. 1. A schematic diagram of the CLAS detector showing, on the left a horizontal section along the beam line, and on the right a section through the target position normal to the beam line.

on electrons, and separating electrons from pions. The unique space and geometry constraints within the CLAS spectrometer require a Cherenkov detector with unusual optical and physical design characteristics.

2. Cherenkov design

The approximately toroidal magnetic field is provided by six superconducting coils spaced by angles of 60° in ϕ, where ϕ is the azimuthal angle around the electron beam. In order to minimize hadron and electron absorption, and secondary particle production upstream of the time-of-flight scintillators and calorimeters, it is necessary to minimize the amount of material in all of the preceding detectors. This places stringent requirements on the physical properties of the Cherenkov detector.

The design of the Cherenkov detector aims at maximizing the coverage in each of the six sectors up to an angle $\theta = 45°$. This is done by covering as much of the available space as possible with mirrors, and placing the light collecting cones and photomultiplier tubes (PMTs) in the regions of ϕ which are obscured by the magnet coils.

Due to the approximately toroidal configuration of the magnetic field, the charged particle trajectories lie approximately in planes of constant ϕ. This suggested that the light collection optics can be designed to focus the light in the ϕ direction. To this end, each of the six sectors was divided into 18 regions of θ, and each θ segment was divided into two modules about the symmetry plane bisecting each sector. This results in a total of 12 identical (except for an inversion symmetry) subsectors around the ϕ direction for each θ interval, and a total of 216 light collection modules.

The optics of each θ module was designed to focus the light onto a photomultiplier tube (PMT) associated with that module and located in the region obscured by the coils. Fig. 2 shows the optical arrangement of one module. The array of the modules in one sector is shown in Fig. 3. The optical elements of each module consist of two focussing mirrors, a "Winston" light collection cone, and cylindrical mirror at the base of the cone as shown in Fig. 2. The light detection is done by means of a 5 in. Phillips XP4500B PMT mounted at the base of the Winston cone.

The trajectory of the light produced by a typical electron passing through the Cherenkov detector is also illustrated in Fig. 2. Since the distance between coils increases approximately linearly with θ, each of the 18 modules in θ has unique optical design parameters.

2.1. Photomultiplier tubes

Monte-Carlo simulation showed that at extreme but important regions of the angular acceptance of the spectrometer the number of detected photoelectrons is rather low. In order to maintain acceptable detection efficiency in these regions, stringent requirements, within budgetary constraints, were placed on the photomultiplier performance. In order to trigger on as few as one photolelectron, the single photoelectron peak has to be clearly resolvable, and as narrow as possible. Likewise, the photoelectron conversion efficiency should be as high as possible at as short wavelengths as possible, since much of the produced Cherenkov light is in the ultraviolet. Also, high photoelectron efficiency should extend over as large an area of the tube's face as possible, since the collected Cherenkov radiation is distributed smoothly over the face of the tube. Given the reflectivity characteristics of the mirrors, and the absorption with wavelength of the radiator gas, as well as budgetary constraints, the Philips XP4500B, with UV glass, proved to be the best match.

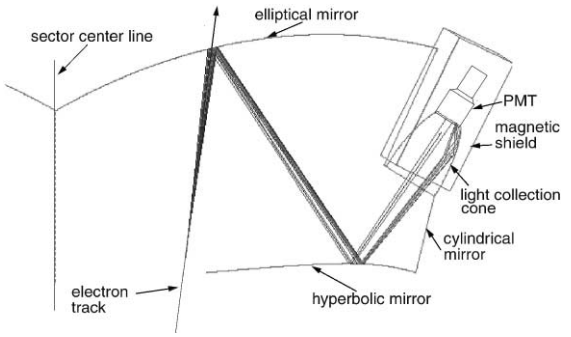

Fig. 2. Optical arrangement of one of the 216 optical modules of the CLAS Cherenkov detector, showing the optical and light collection components. Note that the Cherenkov PMTs lie in the ϕ region obscured by the magnet coils.

2.2. Magnetic shielding

The photomultipliers are located in the fringe field region of the spectrometer coils. It was therefore necessary to surround each PMT with

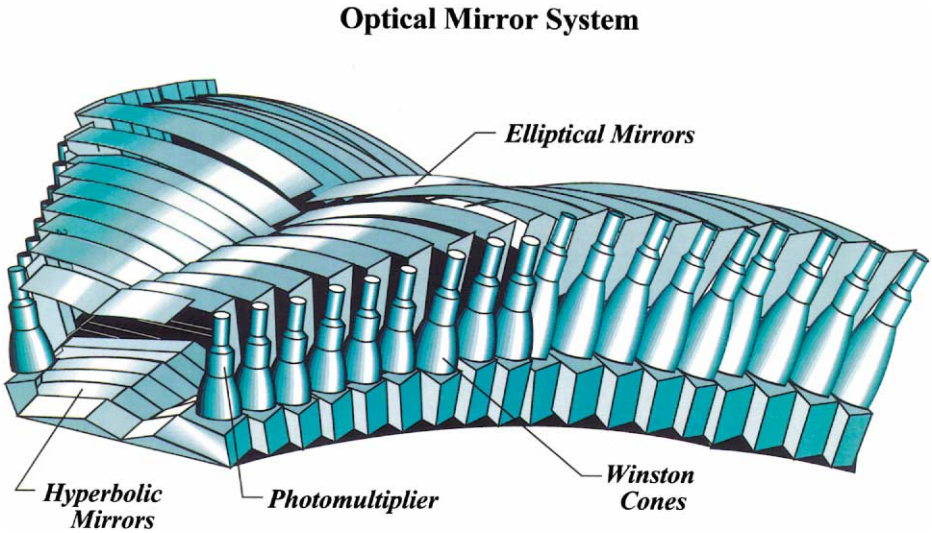

Fig. 3. A schematic diagram of the array of optical modules in one of the six sectors.

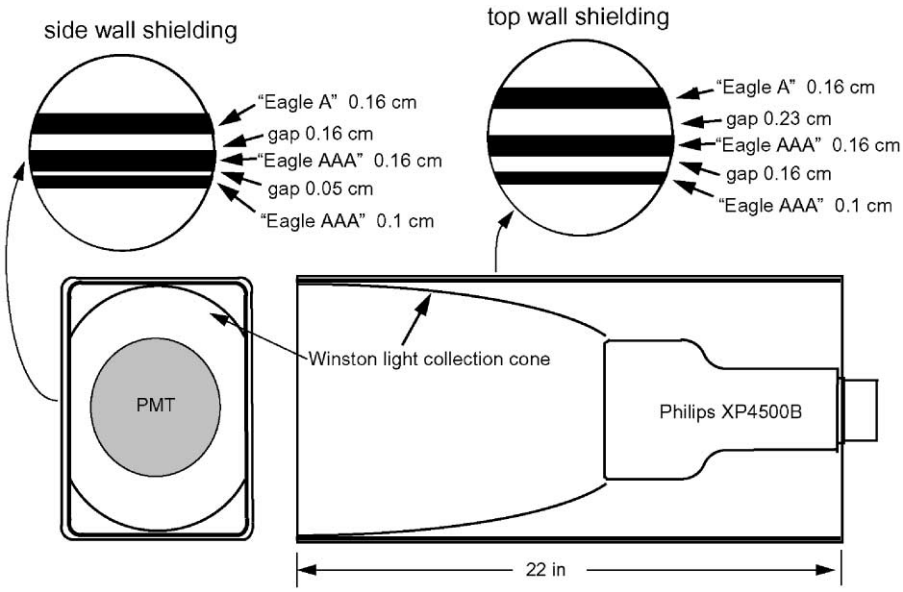

Fig. 4. PMT assembly with Winston light collection cone and magnetic shielding.

high permeability magnetic shields. The magnitude and angle of the applied magnetic field varies widely as a function of PMT position, with the highest fields located at large scattering angles. Computer simulations were used to design a shield that would accommodate components of the applied field up to 11 G parallel to the PMT axis, and 70 G transverse. A diagram of the magnetic shielding is shown in Fig. 4.

The shields and Winston cones were produced in three standard sizes, with the smallest placed at the smallest θ-angle mirror assemblies and the largest at back angles. The PMT photocathode and first dynode are located near the center of each shield. The shields are formed in three layers of magnetic material, each having a rectangular cross-section. The inner and middle layers are composed of high permeability alloy having a saturation induction of 8500 G (Eagle AAA).[3] The outer layer material, of moderate permeability, had a saturation induction of 21,500 G (Eagle A). The thickness of the shielding materials and the separation gaps between the layers for the side and top walls of the shielding are indicated in the insets of Fig. 4.

Bench tests of a prototype large-angle shield at maximum field showed an attenuation factor of 85 for the axial field and 390 for the transverse field at the photocathode position. Thus, an overall field strength of less than 0.2 G is expected in situ. Further tests with a pulsed photodiode were made to determine the detection efficiency of single photons when a shielded PMT is placed inside the spectrometer. The measured relative efficiency was about 95 percent at maximum field, but became worse at higher applied fields due to saturation of the inner layers of the shield.

In order to understand the response of the complicated optical arrangement of the entire detector great effort was expended in developing an elaborate GEANT based design package [4], which simulated the details of the detector response for charged particles of various momenta and directions. The use of this package was essential in obtaining the optimum shapes and orientations of the various mirror components.

[3] Eagle Magnetic Co., Indianapolis, IN 46224, USA.

2.3. Trigger and readout electronics

The CLAS trigger system is designed as a two-level system. The first level provides fast information from the electromagnetic calorimeter, the Cherenkov detector, and the time-of-flight scintillator system. This information must be available within 200 ns. If the event is retained, a second level, using information from the tracking chambers, makes the decision whether the event should be recorded. During electron beam operation, the Cherenkov detector in coincidence with the calorimeter must provide the level 1 information whether the candidate event contains a scattered electron, and should be recorded.

Fig. 5 shows a schematic diagram of the trigger and readout electronics used for the Cherenkov detector. The anode signals from the 216 photomultipliers are amplified by a factor of 10 in specially designed modules, and split. One part of the split signal is sent to the readout electronics, discussed below. Using the remainder of the signal, the left and right elements of each Cherenkov detector segment are linearly added, and output from the UVA132 module.

These analog outputs are then fed into a second UVA module (UVA133), in which groups of four neighboring Cherenkov detector segments are added together. The purpose of adding the signals together is to allow the experimenter to raise the discriminator threshold to a higher level than would be possible if individual segments were used. By using neighboring segments, we effectively trigger on the integrated Cherenkov signal in a portion of the detector. This results in increased pulse height and avoids reduced efficiency for electrons that deposit their Cherenkov light to more than one detector segment. The number of segments included in the sum was determined by a Monte-Carlo simulation which included the full geometry of the detector. Only one event in 2000 had more than four segments collecting light from the simulated incident electron. The summed groups overlap by two segments; that is, the first sum consists of segments 1–4, the second of 3–6, etc. In this way, the 18 detector segments are covered by eight groups of four overlapping segments each. The UVA133 module then discriminates the resulting signals with two separate thresholds, which are set by CAMAC-programmable digital-to-analog modules. This allows a "low" and a "high" threshold to be applied. The high threshold can be used to reduce the noise in the detector, while the low threshold can be used in a prescaled mode to provide unbiased information. The output of the UVA133 module is fed into the CLAS Level 1 trigger, and to a scaler.

The signal for the readout electronics is sent through a passive splitter (UVA122B). One of the split signals from each PMT is fed into a CAMAC leading edge discriminator whose thresholds are set as a group remotely from the control room. The discriminated signal is input to a LeCroy 1872A FASTBUS TDC, and provides the timing signal for the Cherenkov detector. The TDCs were set to have 50 ps/channel timing resolution. The other signal is brought to a LeCroy 1881 M 12-channel FASTBUS 12-bit ADC, and is used to determine the number of photoelectrons coming from the PMT. The Cherenkov ADC and TDC information is read out together with the data from the other detector components using the CEBAF Online Data Acquisition system (CODA).

3. Construction

3.1. Mirror construction

Due to the detector's position upstream of the TOF scintillator array and electromagnetic calorimeters, the mirrors and their supporting framework are required to be as light as possible. In order to minimize the nonuniform material distribution inherent in any supporting frame, the mirrors are constructed to be intrinsically rigid, as well as lightweight. This was accomplished by means of a multi-layered composite construction illustrated schematically in Fig. 6. The mirror surface is aluminum, vacuum deposited,[4] on a Lexan sheet[5] of thickness 0.76 mm, with a vacuum deposited surface layer of MgF_2 to prevent oxidation. This is laminated to a supporting structure

[4] Liberty Mirror Co., Breckenridge, PA 15014, USA.
[5] Cadillac Plastics and Chemical, Albany, NY, USA.

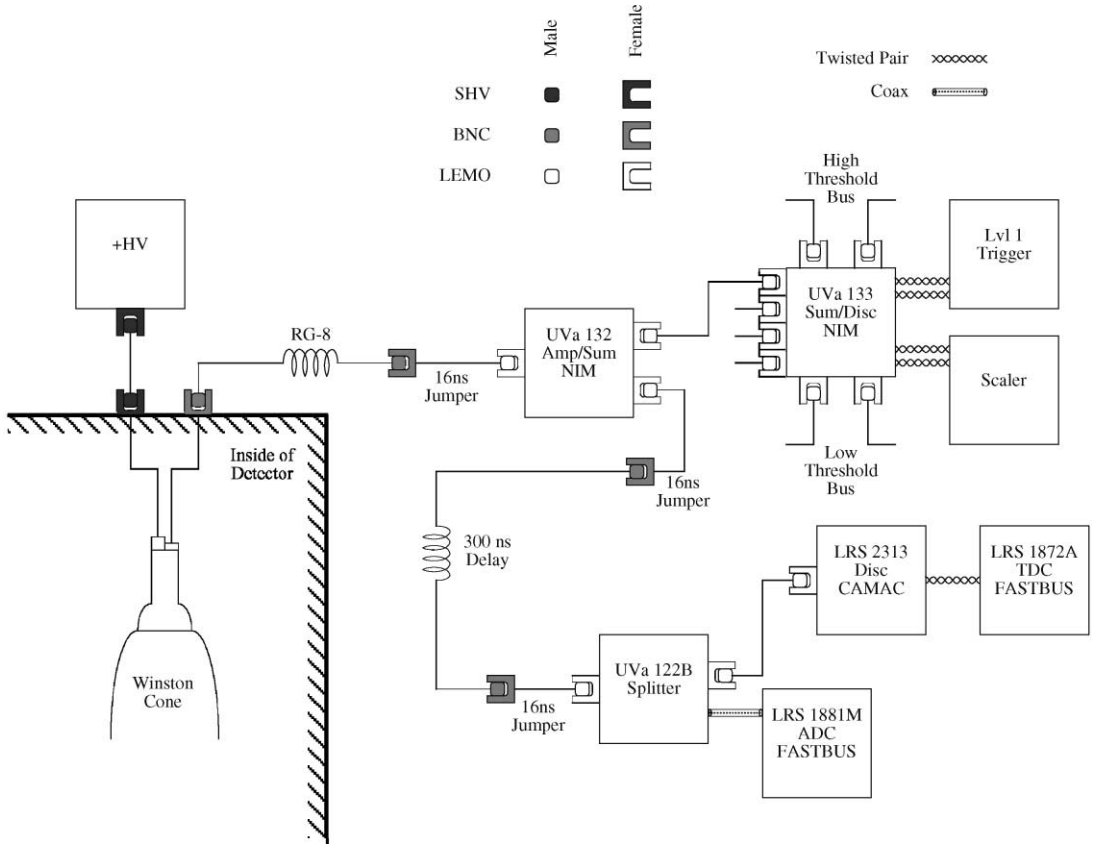

Fig. 5. A schematic diagram of the trigger and readout electronics used for the Cherenkov detector.

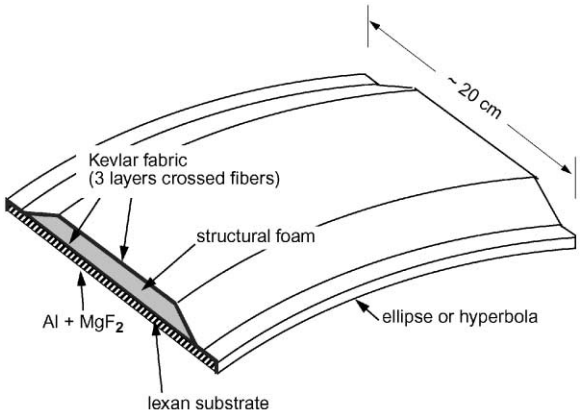

Fig. 6. The cross-section of a mirror used in the CLAS detector.

consisting of three inner and three outer layers of Kevlar,[6] with structural vinyl foam[7] sandwiched between to provide structural rigidity. The Kevlar fabric layers are of density 0.056 g/cm^2, with fibers of successive layers oriented in crossed directions to maximize tensile strength in all directions. Each mirror is supported at one end by an adjustable support frame, illustrated in Fig. 7, which allows complete and independent spatial alignment.

A total of 432 elliptical and hyperbolic mirrors, having 36 different shapes, were fabricated as follows. An aluminum mounting surface having the preset shape of each elliptical or hyperbolic

[6] Fiber Glast Developments Corp., Dayton, OH 45414, USA.

[7] Klegecell type 75 and 45 structural foam. Polinex, Grapevine, TX 76051, USA.

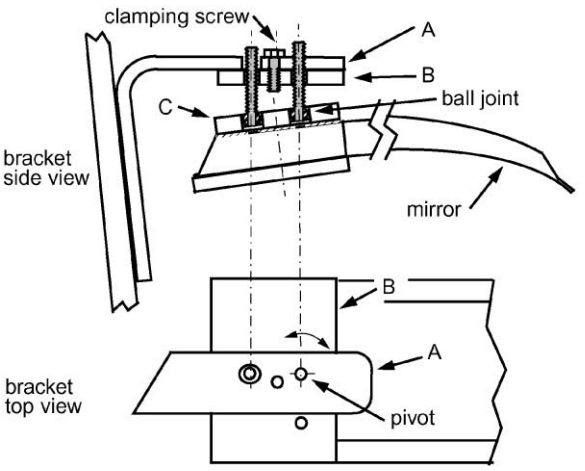

Fig. 7. Detail of the elliptical mirror used in the CLAS Cherenkov detector, showing the mounting/alignment bracket. The bracket used for the hyperbolic mirrors is similar.

mirror is prepared with a PVC anti-bonding coating, followed by a sheet of nylon *peel-ply* to facilitate release of the mirror after fabrication. The aluminized Lexan mirror substrate is placed on the mold, followed by the three inner layers of Kevlar impregnated with Epon (type 828) epoxy. A pre-formed sheet of structural foam was then placed upon the Kevlar. The foam's thickness is tapered down from the supporting end, shown schematically in Fig. 7. The section at the supporting end has a wood inner layer rather than foam to facilitate the attachment of the mounting bracket, as shown in Fig. 7. The foam is of a rigid consistency, which allowed us to pre-form its shape to the mirror curvature by heat treatment, before applying, thus reducing stress after cure. At this stage the structure was covered by plastic vacuum bagging, which was held to the mold and made vacuum-tight by applying a malleable adhesive, and evacuated so that the shape is maintained to that of the mold by air pressure. Cotton bleeder cloth is inserted prior to vacuum bagging to uniformly distribute the evacuation. After a 12 h curing period the three outer Kevlar layers are mounted and again impregnated with epoxy. The entire structure is again evacuated and allowed to cure once more under vacuum for a period of 12 h. The resulting mirrors have a thickness of typically $0.5\,g/cm^2$. The entire mirror assembly is removed and fitted with the supporting frame.

The mirror shapes were optically checked with a specially designed laser system. The reflectivity of the mirrors could not be measured directly due to the large size of a typical mirror assembly. However, small samples were cut from the mirror substrate material corresponding to that used for each individual mirror, and the reflectivity measured for these from the UV through the visible wavelengths. The measured mirror reflectivity are somewhat less than expected for an ideal aluminum surface though typically around 90% in the visible region, and smaller in the near UV (where much of the Cherenkov light is concentrated). The results of a typical measurement are shown in Fig. 8.

The Winston cones used to collect the light onto the PMT surfaces are constructed with flat sides to accommodate close packing, as illustrated in Fig. 4. For fabrication purposes the cones were standardized into three sizes, small, medium and large, of lengths 17, 21, and 29 cm, respectively. The small cones occupied modules 1–10 in each sector, the medium modules 11 and 12, and the

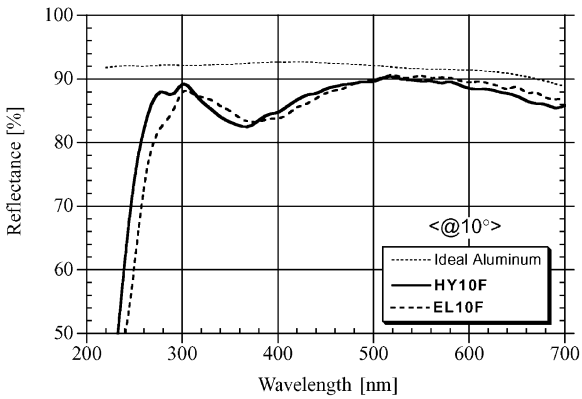

Fig. 8. Measured reflectivity as a function of wavelength for a typical sample of the mirror surface, which consists of Al and MgF_2 successively evaporated onto a substrate of 0.1 in. thickness Lexan sheet. The dotted curve is what would be expected of ideal aluminum. The solid and dashed curves are for the hyperbolic and elliptical mirrors, respectively. The light was incident at an angle of 10° with the normal. Note the suppressed zero on this plot.

large modules 13–18. The small and large cones were fabricated by an electro-forming process.[8] This was the most expensive of the various fabrication methods considered, but offered the best quality surface for mirror deposition, and had the least chance for deterioration over time. It also could be made thinner than with other techniques thereby minimizing the dead wall thickness presented to the reflected light. The copper cones were electro-formed, on pre-shaped steel mandrels, to a nominal thickness of 0.1 cm. The inner surfaces were vacuum coated with aluminum to a thickness of about 40 nm, followed by MgF_2. The small number (24) of medium cones were fabricated from plastic since the high overhead cost for manufacture of the steel mandrel made the cost per cone excessive. The 0.2 in. thick plastic cones were formed by vacuum pressing onto hardwood mandrels, and then were vacuum coated with aluminum and MgF_2 similar to the copper cones. The reflectivity of the cones was checked over the relevant wavelengths and only those passing acceptance criteria were retained. The most important factor leading to lower reflectivity was the nonuniform deposition of MgF_2 onto the inner surfaces.

3.2. Mechanical construction

Due to the six-fold symmetry of the CLAS spectrometer, the Cherenkov detectors were fabricated as six independent identical detector sectors. Each sector subtends an azimuthal angle (ϕ) of 60° and a zenith (scattering) angle $8<\theta<45°$. Each sector was individually assembled.

The superstructure on which all of the detector components, including mirrors, cones, shielding, phototubes and associated cables, were mounted consists of a three walled triangular shaped aluminum frame which forms the outer boundary of each sector.

3.3. Mirror optical alignment

Due to the large size and weight of each module a special mounting fixture was constructed such that assembly and optical alignments were done with the framework positioned in the final orientation of the specific sector. This was done to minimize changes in optics due to changes in gravitational stresses for each orientation of the frame and optical elements during mounting. The assembly and alignment procedure follows.

- The magnetic shields were mounted in their preassigned position on the frame walls. The three frame walls were then assembled to form the detector frame.
- The 36 PMTs were attached to the Winston Cones, and inserted into the magnetic shielding units, and the cylindrical mirrors were attached. The detector frame was then hoisted into the proper position and angle on the mounting fixture.
- The elliptical mirrors were inserted into the detector and aligned using a laser mounted at the putative target position. Fig. 9 illustrates the alignment procedure. The three degrees of freedom were sequentially aligned by means of the specially designed screw-and-ball adjustments built into the mirror mounting brackets. The mirror alignment was performed by using the results of the ray-tracing simulation assuming

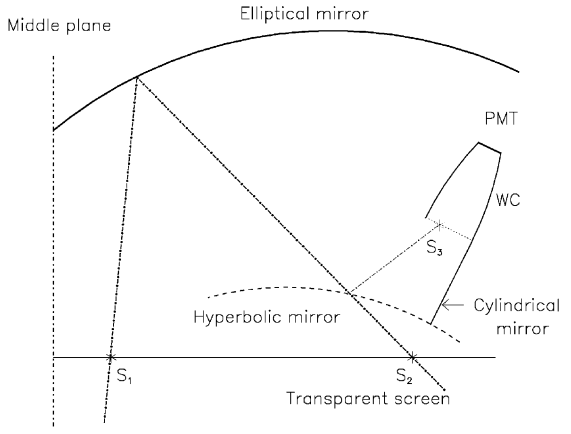

Fig. 9. Illustration of the alignment procedure. First the elliptical mirror is aligned so that the laser light from the target position reflects onto a pre-calculated spot S2 on the transparent mylar screen. Alignment of the hyperbolic mirror requires a secondary reflection onto the predetermined point on a screen located at the face of the Winston light collection cone.

[8] Optical Radiation Corporation, Azuza, CA 91702, USA.

that the Cherenkov light was emitted in exactly the same direction from the target as the electron, with magnetic field turned off so that the electrons would point back to the target. The light reflected from an elliptical mirror intersects a predetermined coordinate on a transparent mylar screen as shown in Fig. 9.

- The hyperbolic mirrors were then mounted, and aligned such that a subsequent reflection of the light from the aligned elliptical mirror was required to intersect a predetermined coordinate on a screen at the entrance to the light collection cone. After alignment, the standard deviation of the distribution of the light on the face of the Winston cone after being reflected from various points on the mirrors was typically about 1 cm, corresponding to an angle of about 1.5 mrad.
- Finally, the elliptical mirror alignment was fixed by permanent attachment with epoxy to a lightweight spine at the midplane of the sector.

3.4. Gas containment windows

After the mirrors were aligned, the detector was removed from the alignment fixture and the gas containment windows were attached. The windows consist of two laminated sheets of Tedlar PVC film[9] of thickness 0.0015 in. each, PVF film sandwiched around a sheet of mylar of thickness 0.003 in. Tedlar was chosen because of its high strength, durability, and opaqueness to light. The window was glued onto the detector walls in a manner which minimizes gas leaks. This was a rather complicated procedure since the windows are not rigid, and the joints with the detector walls must withstand significant forces due to the weight of the C_4F_{10} gas. The gas density of C_4F_{10} is about $9.94\,kg/m^3$. Since each sector has a volume of about $6\,m^3$, the total mass of gas in a sector is about 60 kg, so that the pressure at the joints can be as high as 500 Pa, with transient variations as high as $\pm$ 200 Pa due to variations in external air pressure and ambient temperature. Finally, thin Kevlar sheets, which were securely fastened to the detector frame, covered the entire window area. This was vital to help relieve pressure stresses on the leak-tight window-frame joints. Leak rate, variations in atmospheric temperature pressure, and ambient temperature are monitored continuously.

[9] Tedlar PVF film: Dupont, Wilmington, DE 19898, USA.

3.5. Gas system

C_4F_{10} (perfluorobutane) was chosen as the radiator gas for its high index of refraction ($n = 1.00153$), which results in a high photon yield, and an acceptably high pion momentum threshold of $p_\pi \sim 2.5\,GeV/c$. In addition, C_4F_{10} has excellent light transmission properties. The minimum cutoff wavelength for C_4F_{10} is about 190 nm compared to Freon-12 which is about 230 nm. The measured mirror reflectivity, though typically around 90% in the visible region, drops to about 85% in the near UV, and then typically near 20% at 200 nm, so that light absorption in gas does not play a significant role in the degradation of signal. The physical density of the gas corresponds to about $1\,g/cm^2$ effective thickness traversed by a typical particle.

Each sector of the detector holds about $6\,m^3$ of gas. The cost of the gas for the full detector volume is about \$30 K. With very large joints, where the flexible window attaches to the detector frame, great efforts were employed to minimize gas leaks (see previous section). The high physical density of the gas produces a maximum net pressure of about 340 Pa. Thus, even small leaks result in significant leakage. Finally, a leak rate of about one volume per two years was found to be acceptable.

This gas is supplied to the detector with a gas system built specifically for this purpose. The requirements for such a gas system are that it must be able to recirculate the gas through the detector, maintain an approximately constant pressure within the detector, and remove impurities from the gas. Fig. 10 shows a schematic of the gas system.

Oil bubblers are installed on each sector individually to protect the sector from either an over-pressure or an under-pressure situation. In the event of an over-pressure state, C_4F_{10} is vented to the atmosphere. In an under-pressure condition, air sucked into the detector, both unacceptable

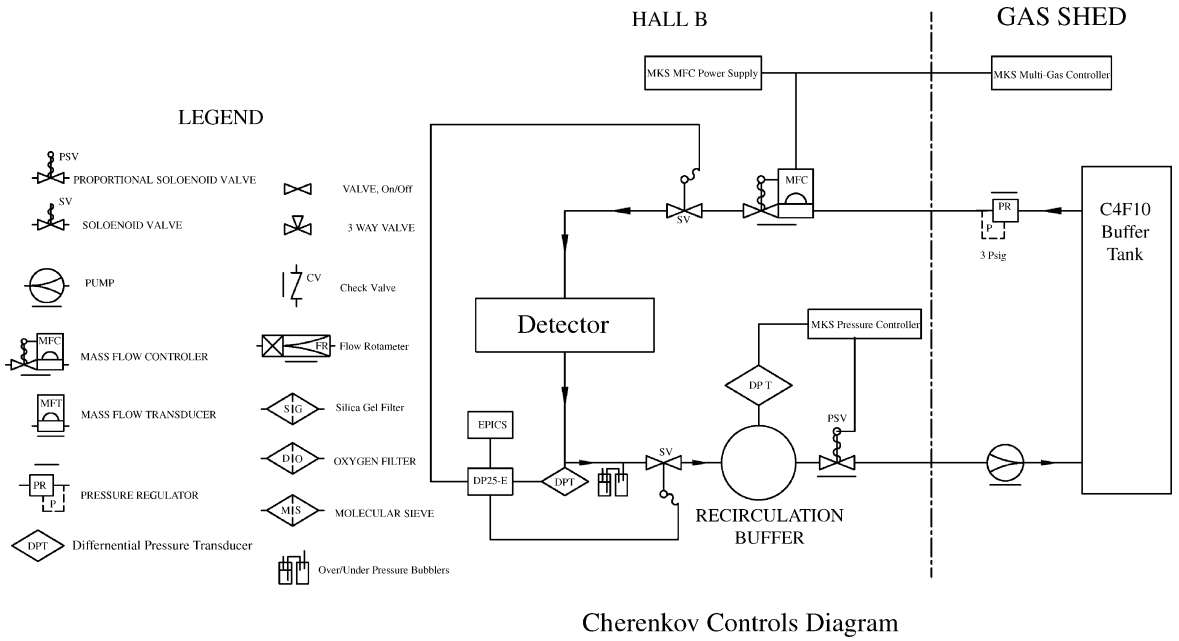

Fig. 10. Schematic diagram of the Cherenkov gas system.

occurances. The gas system is designed to run automatically, altering the flow into and out of the sectors to accommodate changes in external air pressure, with minimal human intervention. Periodic monitoring of the pressure diffierentials within each sector is sufficient to ensure proper functioning of the system.

4. Photomultiplier studies

Measurements of photomultiplier quantum efficiency and photocathode uniformity were accomplished on a custom optical bench designed for the express purpose of performing optical measurements of interest for detector design and testing within the JLAB nuclear physics community. The main mode of testing involved DC measurements of optical response as a function of wavelength. In accordance with this, a standard set of equipment included a UV/VIS broad-band light source (75 W xenon lamp), a UV/VIS monochromator, an integrating sphere and a UV/VIS photomultiplier. The data acquisition process was controlled by a PC. Quantum efficiency (QE) was measured by comparing the response of a sample XP4512B phototube to the measured responses of three different manufacturer-calibrated phototubes. Care was taken to illuminate the entire photocathode with the source light. The manufacturer of the test PMT provided a measure of the QE at 400 nm. Combining this with the measured wave-

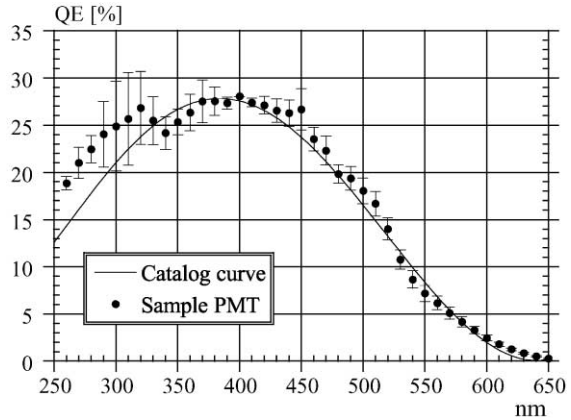

Fig. 11. Typical quantum efficiency data in percent vs. wavelength in nanometer from a selected sample of XP4512B phototubes.

length responses of the test vs. the calibrated PMTs allowed one to calculate the QE for the test PMT. The use of three calibrated phototubes provided an estimate of the errors. Fig. 11 displays a typical example of these data.

These tests also verified that some of the early samples of the phototube used a poorer grade of faceplate leading to insufficient quantum efficiency at the important UV wavelengths, where the Cherenkov spectrum is maximized. Uniformity of response across the photocathode was measured by focussing light (via a silica optical fiber bundle attached to a focussing lens couplet) into a 5 mm spot on the phototube faceplate. The PMT was mounted on a XY scanner which allowed for a raster scan of the PMT photocathode. An example of the DC response (at a typical gain of 2×10^7) for a wavelength of 400 nm is shown in Fig. 12. The central bump is directly above (and due to) the dynode chain. The substantial dip in response across the left half corresponds to a previous observation [5] for this same model of phototube. Analysis by the manufacturer indicated that it is due to a gain drop across the second dynode [5]. Large variations in PMT uniformity (other than this previous dip) were only observed for wavelengths above 600 nm and so were not a problem for this application.

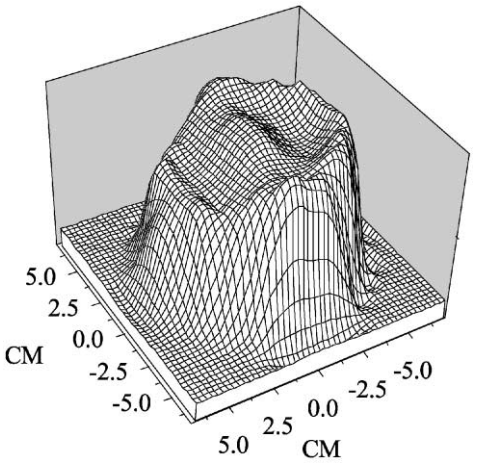

Fig. 12. Typical response of XP4512B across the photocathode. As noted in the text, a major factor in this response curve is the gain behavior of the dynode chain, in particular the second dynode [5].

5. Photomultiplier calibration

The calibration of the CLAS Cherenkov detector consisted of matching the gains of the 216 PMTs. The main reason for this is that the discriminator threshold has the same cutoff for each PMT. This was accomplished by taking a set of special runs in which the data acquisition system was triggered on the PMT noise within the Cherenkov detector, and only the Cherenkov data were written to file. Because the PMTs have different noise rates, from a few hundred hertz to several kilohertz, several runs were necessary, in which the noisier PMTs were turned off.

After all the data were collected, the ADC spectrum for each PMT was fit to a function of the form

$$A(x) = T(A_{\text{noise}}(x) + A_{\text{SPE}}(x)) \tag{1}$$

$$A_{\text{noise}}(x) = C_1 e^{-C_2 x} \tag{2}$$

$$A_{\text{SPE}}(x) = C_3 e^{-(x-C_4)^2/C_5^2} \tag{3}$$

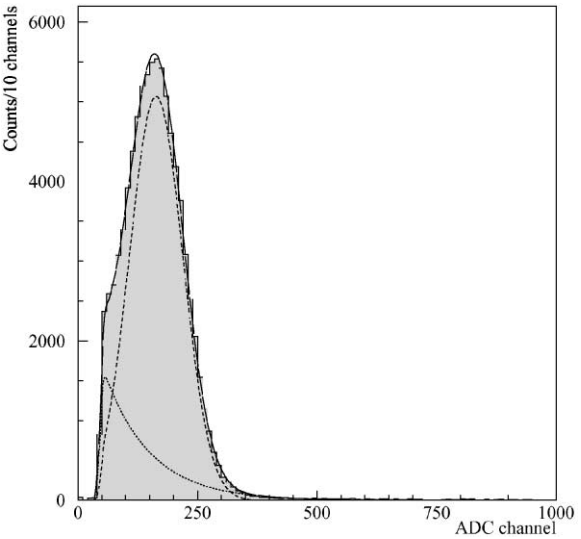

Fig. 13. A typical ADC spectrum showing the single photoelectron peak (dashed line) and the electronic noise (dotted line). The solid curve shows the sum of the two separate components. The PMT threshold is typically approximately 1/4 of the single photoelectron peak position.

where $C_1 - C_5$ are fit constants, and T is a modified step function, smeared to account for the effect of the discriminator threshold used in the trigger. This function presumes that the two main components of the lineshape correspond to electronic noise (A_{noise}) and the single photoelectron peak (A_{SPE}). A typical ADC spectrum is shown along with the fit function in Fig. 13. Using the fit parameters, specifically C_4, which corresponds to the position of the SPE peak, we can adjust the high voltage on the PMT to move the SPE peak into a particular channel.

During the course of the first data run, it was determined that the gains of several of the phototubes drifted with time. To alleviate the trouble this could potentially cause for the data analysis, several calibration runs were taken during the course of the first production experiment.

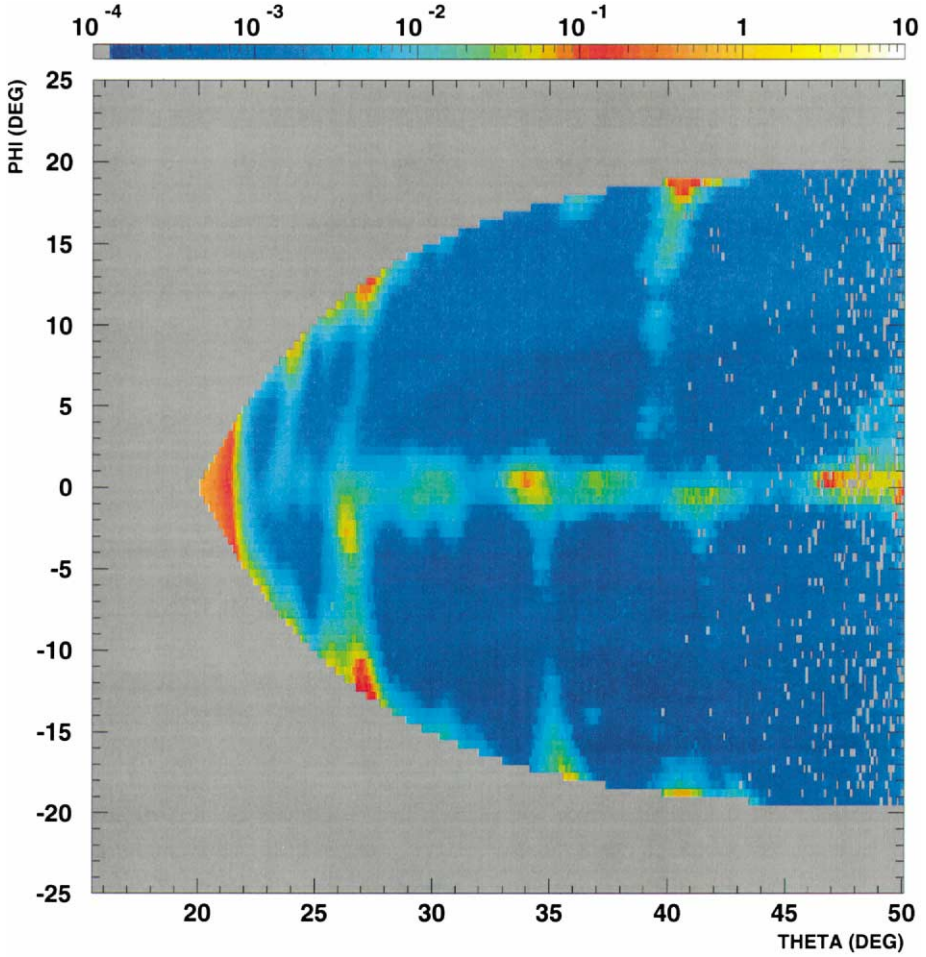

Fig. 14. Acceptance of the CLAS Cherenkov detector for one of the six sectors measured using 1.6 GeV electrons elastically scattered from protons. Plotted are scattering angles θ and ϕ defined with respect to the beamline. The inefficiency (1–efficiency) is plotted according to the color scale at the top of the figure. The number of events per bin is logarithmically weighted according to the color scale at top. The dark blue regions which dominate the plot correspond to between 0.001 and 0.02. The sharp edges correspond to the software fiducial cuts discussed in the text. For this measurement the magnetic field was set to 60% of its maximum value. The scattering angles θ and ϕ are defined with respect to the beamline.

By monitoring the gain drift over time, we can get a good idea of its effect on our data.

6. Performance

6.1. Fiducial volume and efficiency

In order to calculate absolute cross-sections, both the fiducial volume of the CLAS and the detector efficiency within that volume must be established. Because of the open geometry of the CLAS, particles can trigger the detector at the extreme edges of the acceptance, where the detector efficiency may not be well understood. Therefore, the fiducial boundary which defines "good" acceptance must be carefully determined for each detector component, in order to produce a well-defined solid angle and minimize large efficiency corrections.

For the Cherenkov detector, this boundary is defined by the edges of the mirrors, beyond which the optical collection efficiency for Cherenkov light rapidly drops. This efficiency was studied in situ using elastic scattering of electrons from a hydrogen target. The strong kinematic correlation

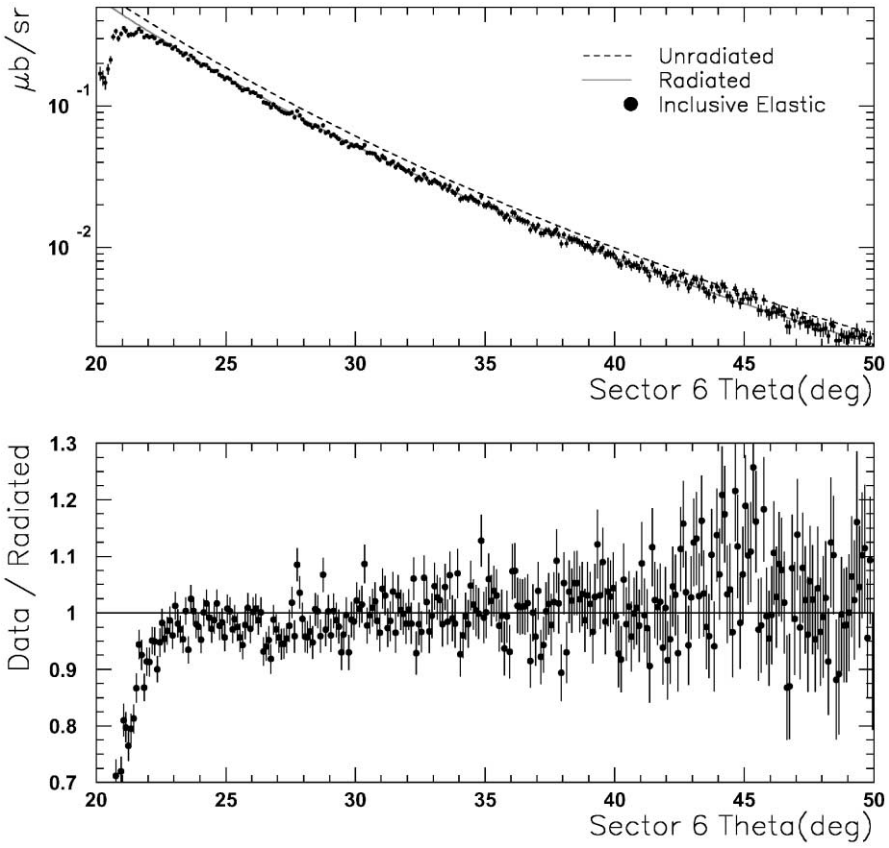

Fig. 15. (Top): Measured cross-section for ep → ep elastic scattering at beam energy of 1.645 GeV. Fiducial cuts for the Cherenkov detector, shown in Fig. 14, are used to define the solid angle for each θ bin. *No corrections* for the Cherenkov efficiency were made. The curve labeled "Radiated" denotes the Rosenbluth formula, radiatively corrected according to Mo and Tsai [6], with the elastic form factor parameterization of Bosted [7]. The large discrepency at $\theta < 23^\circ$ is in a region where the Cherenkov inefficiency becomes relatively large and less reliable (see Fig. 14). (Bottom): The ratio of the radiatively corrected measured cross-section to that calculated with the Rosenbluth formula.

between scattering angle and momentum for elastic events creates a one-to-one correspondence between the electron's azimuthal and polar angles at the target (θ, ϕ), and the entry point of the electron on the surface of the Cherenkov detector.

Elastically scattered electrons are selected by kinematical cuts, and a match between a reconstructed track and a reconstructed shower in the electron calorimeter. A cut on the invariant mass of the hadronic final state, $W^2 = (E - E')^2 - (\boldsymbol{P} - \boldsymbol{P}')^2$, is used to select elastic events.

The Cherenkov inefficiency as determined from the measured photoelectron yield is plotted in Fig. 14. Here, variations in the optical collection efficiency associated with the individual mirror segments are apparent. Except for isolated spots at the midplane, where the gaps between mirrors are largest, the electron efficiency within the fiducial acceptance should exceed 99%.

Outside of the region of high optical collection efficiency, the photoelectron inefficiency increases rapidly, and this region must be excluded using fiducial cuts. Using only the events within this fiducial boundary, we have calculated raw elastic cross-sections, shown in Fig. 15.

These show deviations from the expected dependence that are no greater than $\pm$ 5%, except at the smallest angles ($\leqslant 22^\circ$), where the fiducial cut extends beyond the edge of the forward most mirror.

7. Conclusion

The spatial configuration of the toroidal spectrometer CLAS required the design, construction and deployment of a large gas Cherenkov detector with a complex optical configuration. The detector has been shown to have a large efficiency and meet design specifications of inefficiency less than 0.5% over most of the forward angular acceptance available to CLAS for electron detection.

Acknowledgements

The authors acknowledge the continuous positive support of Bernhard Mecking, Hall B leader. Thanks are also due to John O'Meara, Hall B chief engineer, for his guidance during the early stages of the project.

References

[1] D.S. Carman et al., Nucl. Instr. and Meth. A 419 (1999) 315; Nucl. Instr. and Meth. A 449 (2000) 81.
[2] E.S. Smith et al., Nucl. Instr. and Meth. A 432 (1999) 265.
[3] M. Amarian et al., Nucl. Instr. and Meth. A 460 (2001) 239.
[4] CERN Program Library 2123.
[5] M. Moszynski et al., Nucl. Instr. Meth. A 307 (1991) 97.
[6] L.W. Mo, Y.S. Tsai, Rev. Mod. Phys. 41 (1969) 205.
[7] P.E. Bosted, Phys. Rev. C 51 (1995) 409.